International Journal of Thermophysics, Vol. 27, No. 5, September 2006 (© 2006)
DOI: 10.1007/s10765-006-0108-4

Deriving Analytical Expressions for the Ideal Curves and Using the Curves to Obtain the Temperature Dependence of Equation-of-State Parameters

G. A. Parsafar[1,2] and C. Izanloo[1]

Received September 15, 2005

Different equations of state (EOSs) have been used to obtain analytical expressions for the ideal curves, namely, the Joule–Thomson inversion curve (JTIC), Boyle curve (BC), and Joule inversion curve (JIC). The selected EOSs are the Redlich–Kwong (RK), Soave–Redlich–Kwong (SRK), Deiters, linear isotherm regularity (LIR), modified LIR (MLIR), dense system equation of state (DSEOS), and van der Waals (vdW). Analytical expressions have been obtained for the JTIC and BC only by using the LIR, MLIR, and vdW equations of state. The expression obtained using the LIR is the simplest. The experimental data for the JTIC and the calculated points from the empirical EOSs for the BC are well fitted into the derived expression from the LIR, in such a way that the fitting on this expression is better than those on the empirical expressions given by Gunn et al. and Miller. No experimental data have been reported for the BC and JIC; therefore, the calculated curves from different EOSs have been compared with those calculated from the empirical equations. On the basis of the JTIC, an approach is given for obtaining the temperature dependence of an EOS parameter(s). Such an approach has been used to determine the temperature dependences of A_2 of the LIR, a and b parameters of the vdW, and the cohesion function of the RK. Such temperature dependences, obtained on the basis of the JTIC, have been found to be appropriate for other ideal curves as well.

KEY WORDS: Boyle curve; ideal curves; equation of state; Joule–Thomson inversion curve; linear isotherm regularity; modified linear isotherm regularity.

[1] Department of Chemistry, Sharif University of Technology, P.O. Box 11365-9516, Tehran, Iran
[2] To whom correspondence should be addressed. E-mail: Parsafar@sharif.edu

1. INTRODUCTION

An ideal curve is a curve along which one property of a real fluid is the same as that property for the hypothetical ideal gas at the same temperature (T) and density (ρ). Based on this very general definition, ideal curves can be defined for almost every property, but usually only for the unit compressibility factor (Z) and zero value for its first derivatives [1]. Brown [2] described the ideal curves and called them characteristic curves along which certain thermodynamic properties of the fluid agree with those of the perfect gas.

The ideal curves are useful as criteria for assessing the extrapolation behavior of equations for simple substances, because they contain important information on the behavior in the high-temperature, high-pressure region. Furthermore, these curves establish limiting conditions, which may be useful for extrapolations. De Reuck [3] discussed the usefulness of these characteristic (ideal) curves for extrapolating an equation of state (EOS).

The oldest empirically known ideal curve is the Zeno line or the $Z=1$ contour. The density of many fluids along the Zeno line has been found to be nearly a linear function of temperature. The $Z=1$ contour was first discovered by Batchinski [4] in 1906. Among the diverse names used are the orthometric condition, ideal-gas curve, and finally the term Zeno line was adopted by Xu and Herschbach [5]. During the late 1960s, Holleran [6–9] proposed several useful applications for the $Z=1$ contour. In recent years, from molecular-dynamics simulations, Herschbach [5] obtained a Zeno line close to experimentally measured values over a wide range of densities by using the Lennard–Jones potential, simple point charge (SPC), and extended SPC (SPC/E) models for pure water.

The behavior of ideal curves may be considered as a rigorous criterion for the accuracy of an EOS [1]. Parsafar and Saydi [10] made such a study of the Zeno line. They showed that only the van der Waals (vdW) EOS is able to predict a linear relation between the density and temperature on the $Z=1$ contour. However, the resulting line is quite different from that of experiment. They obtained the temperature dependences of the a and b parameters in such a way that experimental pvT data fitted well onto the EOS. Considering such temperature dependences for the a and b parameters leads to a line closer to the experimental $Z=1$ contour. However, the resulting curve is not quite linear anymore.

Polishuk and Vera [11] discussed that it is not an easy task to develop a van der Waals-like EOS with a theoretically correct hard-sphere or hard-body repulsive term that could simultaneously give an accurate representation of vapor pressures and densities of real fluids, without making its parameters strongly temperature dependent.

The Joule–Thomson inversion curve (JTIC) is the locus of thermodynamic states in which the temperature of a fluid does not change upon isenthalpic expansion or the locus of points at which the Joule–Thomson coefficient (μ_{JT}) is zero:

$$\mu_{JT} \equiv \left(\frac{\partial T}{\partial p}\right)_h = 0. \tag{1}$$

The inversion criterion, Eq. (1), may be written in several alternative forms. For pressure we may use

$$T\left(\frac{\partial p}{\partial T}\right)_\rho - \rho\left(\frac{\partial p}{\partial \rho}\right)_T = 0 \tag{2}$$

and for the compressibility factor, one may use

$$\left(\frac{\partial z}{\partial T}\right)_p = 0. \tag{3}$$

The JTIC was also called the Charles curve by Brown. The JTIC is the best criterion for evaluating an EOS over a wide range of temperature and pressure [12–14]. Dilay and Heidemann [12] studied the JTIC using the Soave–Redlich–Kwong (SRK), Peng-Robinson, perturbed hard-chain, and Lee-Kesler EOSs. Juris and Wenzel [15] compared the experimental JTIC with those calculated from the vdW, Deiters, Berthelot, Redlich–Kwong (RK), truncated virial (with the second and third virial coefficients taken from the Pitzer and Chueh–Prausnitz correlations), Su–Beattie–Bridgeman, several reduced forms of Benedict–Webb–Rubin, and Martin–Hou EOSs. Darwish and Al-Muhtaseb [16] calculated the JTIC using the modified PR by Melhem et al., Trebble-Bishno, and Jan-Tsai EOSs. Maghari and Seyed Matin [17] calculated the JTIC by using Adachi–Lu–Sugie, Kubic–Martin, Yu–Lu, and Twu–Coon–Cunningham EOSs. The LIR was used to investigate the JTIC [18]. Heyes and Liaguno [19] applied molecular simulation for determining the JTIC for the Lennard–Jones fluid. Colina et al. [20] simulated the JTIC for CO_2 using two different approaches based on Monte Carlo simulation for the isothermal–isobaric ensemble.

Much effort has been made to obtain a universal expression for the JTIC from the available experimental data of light fluids. Gunn et al. [21] calculated inversion points from volumetric data of Ar, CO, CH_4, C_2H_6, N_2, and Xe with the second and third virial coefficients based on the Kihara intermolecular potential. Gunn et al. [21] calculated some additional theoretical points for Ar using a truncated virial EOS. All of

the available inversion points, including the calculated and experimental points, were fitted with the following empirical equation:

$$p_r = \sum_{i=0}^{5} a_i T_r^i, \tag{4}$$

where $p_r = p/p_c$ and $T_r = T/T_c$ are the reduced pressure and temperature and a_i are constant coefficients independent of the molecular identity. It was also found that Eq. (4) is appropriate only for simple and spherical molecules. It was also found that the coefficients in Eq. (4) could be generalized for hydrocarbon and non-hydrocarbon materials (excluding alcohols), in the reduced form [22],

$$a_i = a_i^{(0)} + a_i^{(1)}\omega^n \qquad 0.85 \leqslant T_r \leqslant 4.5, \tag{5}$$

where ω is the acentric factor and values of n and a_i depend on the molecular identity.

A relatively simpler equation based on the available Joule–Thomson inversion data of Ar, NH_3, CO_2, CO, CH_4, C_2H_6, N_2, and C_3H_8 was proposed by Miller [13] as

$$p_r = a + \frac{b}{T_r} + cT_r^2. \tag{6}$$

In spite of available empirical Eqs. (4–6), an analytical expression for the JTIC has not been presented based on any EOS. One purpose of this work is to obtain an analytical equation for the JTIC, using different EOSs.

The Boyle curve (BC) is a curve on which the fluid obeys Boyle's law. This curve is characterized by the following equation:

$$\left(\frac{\partial z}{\partial V}\right)_T = 0 \tag{7}$$

or equivalently,

$$\left(\frac{\partial p}{\partial v}\right)_T = -\frac{p}{v}. \tag{8}$$

This curves lies completely inside the JTIC.

The Joule inversion curve (JIC) was also called the Amagat curve by Brown [2]. It is characterized by the following expression:

$$\left(\frac{\partial z}{\partial T}\right)_v = 0 \tag{9}$$

or equivalently,

$$\left(\frac{\partial p}{\partial T}\right)_v = \frac{p}{T}. \tag{10}$$

The temperature and pressure range of this curve is so vast that it encloses both the JTIC and BC. On this curve, the Joule coefficient, $\mu_J = \left(\frac{\partial T}{\partial v}\right)_E$, is equal to zero, where E is the internal energy. Since experimental data have not been reported for the JIC and BC, we shall use different EOSs to calculate such curves and compare the results with those obtained from empirical equations [23–26].

The other purposes of this work are to use different EOSs to (1) obtain analytical expressions for both the Boyle and Joule ideal curves, (2) search for the ability of different EOSs to predict the ideal curves, and finally (3) to present an approach for which the parameters of an EOS are obtained in such a way that it gives better predictions for the ideal curves than its original form.

2. DERIVING AN ANALYTICAL EXPRESSION FOR THE JTIC VIA DIFFERENT EOSs

We have selected seven EOSs to calculate the JTIC. These EOSs are the RK, SRK, Deiters, LIR, modified LIR (MLIR) by Parsafar and Saydi [10], dense system equation of state (DSEOS), and vdW EOS that are given in the Appendix.

In the LIR, the A and B parameters are temperature dependent as

$$A = A_2 - \frac{A_1}{RT}, \qquad B = \frac{B_1}{RT}, \tag{11}$$

where A_1 and B_1 are constants which depend on the attractive and repulsive terms of the average effective pair potential [27, 28], respectively, A_2 is related to the non-ideal thermal pressure, and R is the gas constant. The combination of the LIR with $Z = 1$ does not lead to a linear relation between ρ and T. Therefore, the LIR in its original formulation does not predict the $Z = 1$ contour if A_2 is considered to be a constant. However, it was shown that if A_2 is temperature dependent as

$$A_2 = a + bT_r + c/T_r, \tag{12}$$

where $a = -2\alpha\beta B'/R$, $b = -\beta^2 B'/R$, and $c = A'/R - \alpha^2 B'/R$, and α, β, B', and A' are constant parameters that depend on the selected fluid, then the LIR can predict the Zeno line [10]. We shall refer to the LIR with the

temperature dependence of A_2 given in Eq. (12) as the MLIR from now on.

The simultaneous solution of Eq. (2) with any EOS will provide us the locus of points for which μ_{JT} is zero. The calculated JTIC for Ar, N_2, and CO_2 are shown in Fig. 1 by using different EOSs. As shown in Fig. 1, the calculated points given by the Deiters EOS are well-matched with experimental points at low temperatures and at the top of the curve. Actually all the EOSs give good predictions for the JTIC at low temperatures, except for the vdW. However, the differences among the predictions of different EOSs with experimental values are significant around the maximum and also at high temperatures. As one may expect, the LIR and DSOES give satisfactory results only at high densities for which they are valid ($\rho > \rho_B$, where ρ_B is the Boyle density).

The JTIC predicted by complex multi-parameter EOSs, namely, those of Pitzer and Span–Wagner, are also given in Fig. 1a. The prediction of the Span–Wagner EOS is excellent for the entire temperature range. However, the Pitzer EOS prediction is poor at high temperatures, which is due to the physically erroneous prediction of the third virial coefficient [29]. At low but finite densities, the JTIC is governed by a combined function of the second and third virial coefficients [29]. It follows that any EOS that fails to predict the third virial coefficient accurately will yield an inaccurate JTIC, at least, at very high temperatures. Even if the second virial coefficient is well represented and the predicted curve terminates at the correct endpoint, it will approach this point from an incorrect direction, i.e., with the wrong slope, and possibly, curvature, due to the inaccurate third virial coefficients [29].

The maximum along the JTIC and its corresponding temperature, along with the maximum of the inversion temperature (when $p \to 0$) for CO_2 are given in Table I, using different EOSs. We have been able to obtain analytical expressions for the JTIC by using the LIR, MLIR, and vdW EOSs, which are given in Table II. The expression for the LIR may be simply written as

$$p = \frac{(aT^3 + bT^2 + cT + d)}{(eT + f)^{1/2}}. \tag{13}$$

The JTIC experimental data for CO_2 [30] were fitted with Eq. (13) and also with the empirical Eqs. (4) and (6). The results are shown in Fig. 2; the correlation coefficients for Eqs. (13), Miller, and Gunn et al. are equal to 0.999, 0.993, and 0.998, respectively.

Most of the EOSs considered in this work are not able to predict well the upper temperature branch of the JTIC (see Fig. 1). We suspect that

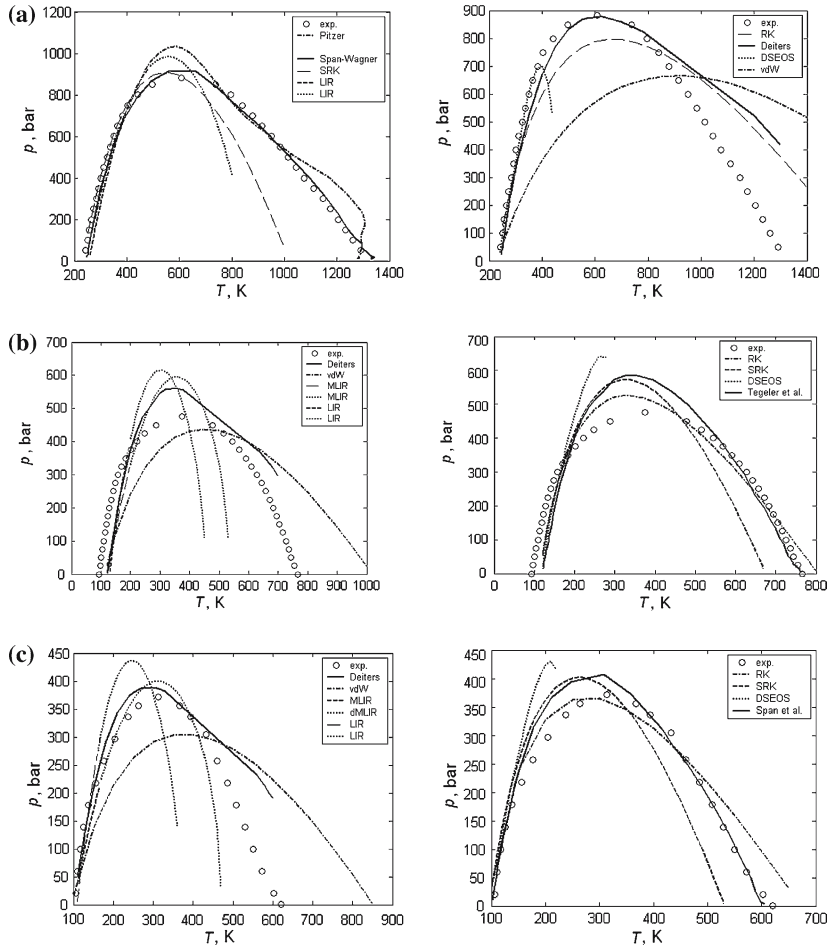

Fig. 1. Predicted JTIC by different EOSs compared with experimental data for (a) CO_2 [30], (b) Ar [12], and (c) N_2 [30]. For the LIR, the dotted curve has a density less than the Boyle density for which the equation is not valid.

this problem is due to the inaccuracy of the EOSs at high temperatures. To investigate such inaccuracy, we have calculated the pressure using the RK EOS for CO_2 as an example, and compared the results with experimental values [30]. The comparison is shown in Fig. 3 for CO_2. It is evident from Fig. 3 that the RK EOS predicts the upper temperature branch even more accurately than the lower one, so our suspicion is not reasonable. Therefore, we should search for another reason.

Table I. Temperature and Pressure at the Maximum of the JTIC and its Maximum Inversion Temperature for CO_2, Predicted from Different EOSs

EOS	Coordinates of Maximum		Maximum Inversion Temperature (K)
	Pressure (bar)	Temperature (K)	
RK	793.96	669.67	1577.53
SRK	912.10	547.30	1003.69
Deiters	887.59	621.71	1499.18
LIR	984.91	545.22	817.82
MLIR	665.22	366.47	621.20
vdW	665.10	912.63	2053.42
DSEOS	640.11	390.08	475.36
Pitzer	1105.86	607.64	1304.67
Span–Wagner	905.30	585.26	1353.33
Miller equation	870.06	681.17	1515.60
Experimental values	895.15	603.88	1378.70

Table II. Analytical Expressions for the JTIC by using the LIR, MLIR, and vdW EOSs

EOS	Expressions for the JTIC
LIR	$p=\dfrac{(-25B_1RT+6A_2^2R^2T^2-13A_2RTA_1+6A_1^2)(2A_2RT-3A_1)\sqrt{5}}{125B_1\sqrt{-(2A_2RT-3A_1)B_1}}$
MLIR	$p=(4b^2R^2T^4+11bR^2aT^3+(6a^2R^2-14bRA_1+14bR^2c)T^2+(13aR^2c-25RB_1-13aRA_1)T+6c^2R^2-12cRA_1+6A_1^2)(bRT^2+2aRT+3cR-3A_1)\sqrt{5}/(125B_1\sqrt{-(bRT^2+2RaT+3cR-3A_1)B_1v_c})$
vdW	$p=-\dfrac{(RTb-2a)a(2aRTb+5RTb\sqrt{2}\sqrt{aRTb}+3R^2T^2b^2-2a\sqrt{2}\sqrt{aRTb})}{b^2(\sqrt{2}\sqrt{aRTb}+RTb)(2a+\sqrt{2}\sqrt{aRTb})^2}$

There are not many data for the JTIC. Some reported values of μ_{JT} have been obtained by appropriately differentiating pvT data [13]. Nain and Aziz [31] predicted the μ_{JT} for the noble gases at zero pressure on the basis of numerous intermolecular potentials. The JTIC can be obtained by plotting Z against T for isobars to obtain their extrema [32]. These minimum and maximum points are the inversion points that belong to the lower and upper branches of the JTIC, respectively. We have plotted such a curve for the 550 bar isobar of CO_2 in Fig. 4a, b.

In principle, we may use a similar approach to plot other ideal curves using pvT data. For instance, if we plot Z versus T for an isochore, we

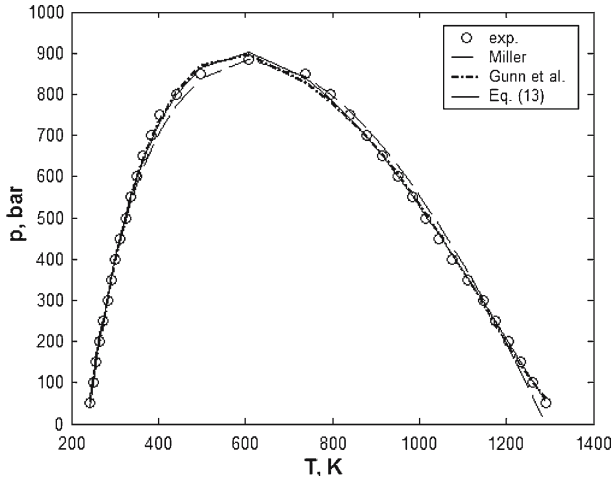

Fig. 2. Experimental data of the JTIC for CO_2 are fitted with Eqs. (4), (6), and (13).

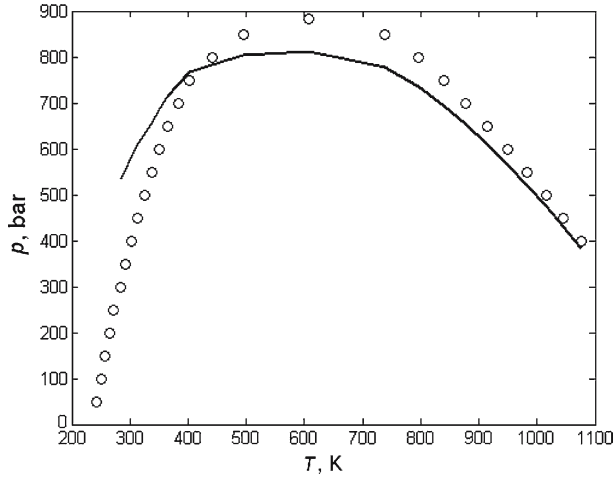

Fig. 3. Calculated pressure given by the RK EOS is compared with experimental values of JTIC for CO_2 [30].

may obtain two points of the BC from its extrema. Such a task was done for the $15\,mol{\cdot}L^{-1}$ isochore of CO_2 in Fig. 4c. As shown in this figure, the minimum in this curve is obvious, but the maximum is beyond the available experimental data. For the JIC, we may plot Z versus p for an isotherm (see Eq. (9)) from which two points of the curve may be obtained.

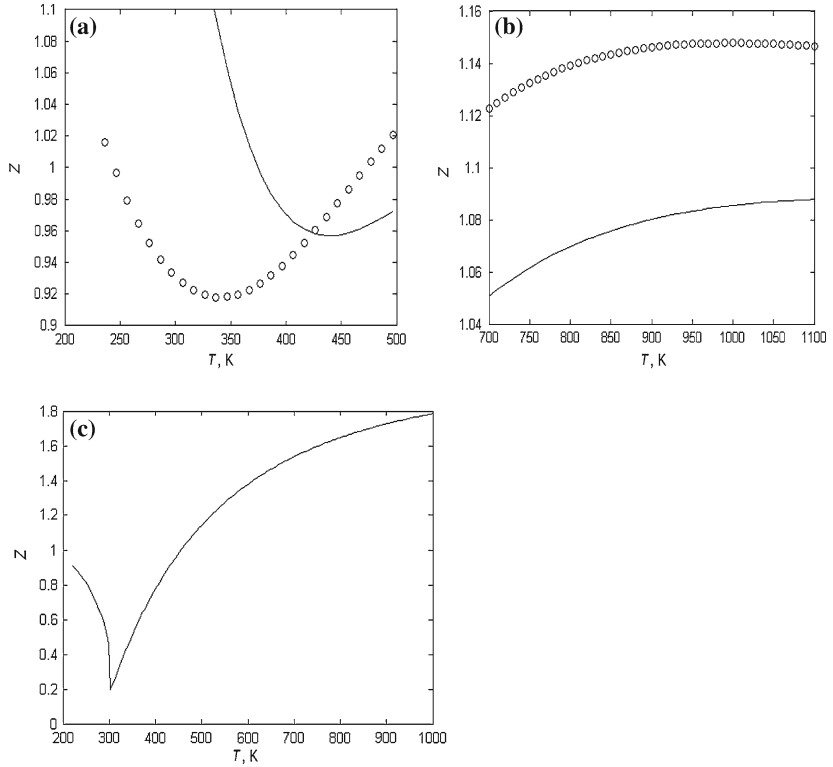

Fig. 4. An isobar (550 bar) for CO_2 using experimental pvT data [35] to obtain (a) the minimum and (b) the maximum, which are two points of the JTIC; (c) a similar plot for the 15.0 mol · L^{-1} isochore of CO_2.

However, the temperature and pressure ranges of the curve are so vast that no experimental data are available to obtain such points. Therefore, the available experimental pvT data are only appropriate to obtain the JTIC. As shown in Fig. 4a, b, the minimum point of the RK EOS is reasonable, compared to that of experiment. However, its maximum point is far beyond the experimental value. Therefore, we may expect that the RK EOS is more accurate for prediction of the lower temperature branch than the upper one of the JTIC.

3. DERIVING AN ANALYTICAL EXPRESSION FOR THE BC VIA DIFFERENT EOSs

Equation (8) gives the condition for the BC. This curve is also the curve on which the fluid obeys Boyle's law or, in other words, the pressure

Table III. Analytical Expressions for the BC by using the LIR, MLIR, and vdW EOSs

EOS	Expressions for the BC
LIR	$p=\dfrac{(-4B_1RT+A_2^2R^2T^2-2A_2TRA_1+A_1^2)(A_2RT-A_1)\sqrt{2}}{8B_1\sqrt{-(A_2RT-A_1)B_1}}$
MLIR	$p=(b^2R^2T^4+2aR^2bT^3+(a^2R^2+2bR^2c-2bRA_1)T^2+(2aR^2c-4B_1R-2aRA_1)T$ $+c^2R^2-2cRA_1+A_1^2)(aRT+bT^2R+cR-A_1)\sqrt{2})$ $/(8B_1\sqrt{-(aRT+bRT^2+cR-A_1)B_1v_c})$
vdW	$p=-\dfrac{(-a+RTb)a(3RTb\sqrt{aRTb}+2R^2T^2B^2-a\sqrt{aRTb})}{b^2(\sqrt{aRTb}+RTb)(a+\sqrt{aRTb})^2}$

is proportional to density for any isotherm. The simultaneous solution of Eq. (8) with any EOS will provide the locus of points for which the fluid obeys Boyle's law.

For the BC, no experimental data are reported, so we may use an empirical EOS, which is typically designed for vast ranges of temperature and pressure for a fluid, to obtain the curve. The results of such calculations are given in Fig. 5 for Ar, N_2, and CO_2 by using different EOSs. We have been able to obtain analytical expressions for the BC by using the LIR, MLIR, and vdW EOSs, which are given in Table III. Among such expressions, the simplest one is that obtained from the LIR, which may be simply presented by Eq. (13). As shown in Fig. 6, the calculated points of the BC from the empirical EOS are well fitted with Eq. (13) for Ar and N_2.

4. DERIVING AN ANALYTICAL EXPRESSION FOR THE JIC VIA DIFFERENT EOSs

For the JIC, no experimental data are reported, so we may use an empirical EOS to obtain this curve. The results of such calculations show that most of the EOSs considered in this work do not give appropriate expressions for the JIC; see Table IV. However, some of these, including Deiters and the DSEOS, numerically predict this curve that is shown in Fig. 7 and the MLIR gives an analytical expression. As shown in this figure, the deviations from the curves calculated from the empirical equations are significant. (Note that the density range, in which the DSEOS and MLIR are valid, is very limited in comparison with the temperature range shown in Fig. 7.)

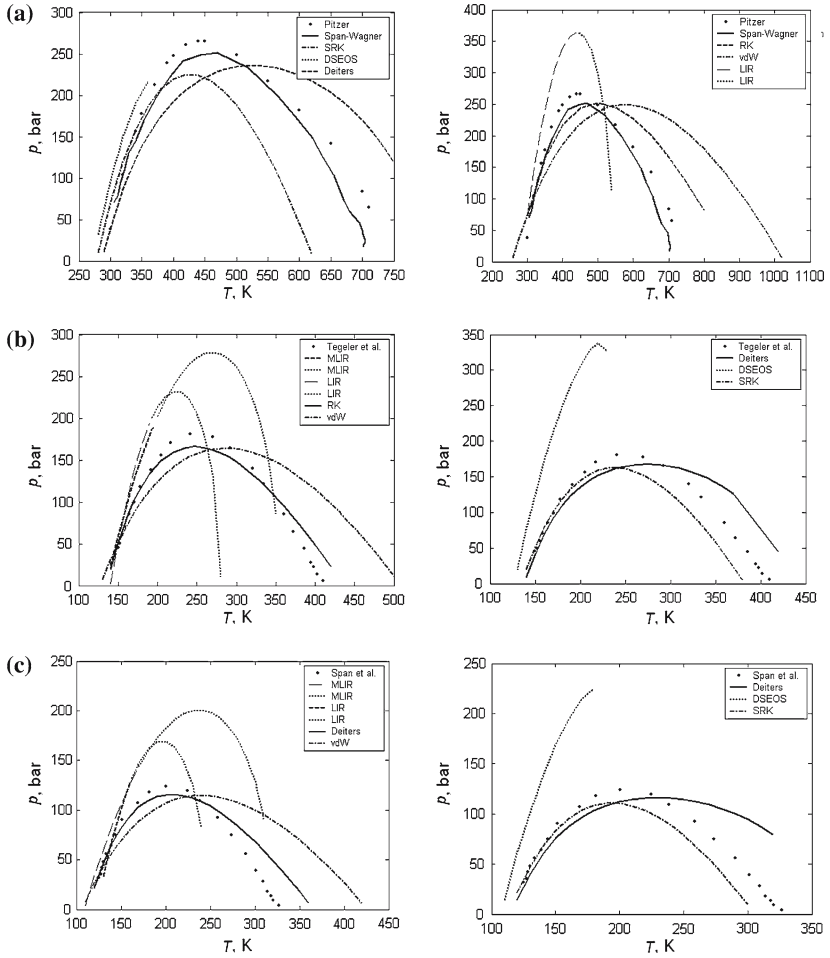

Fig. 5. Predicted BC by using different EOSs compared with calculations using the empirical equation for (a) CO_2 (Pitzer [24] and Span–Wagner [23]), (b) Ar (Tegeler et al. [26]), and (c) N_2 (Span et al. [25]).

5. TEMPERATURE DEPENDENCE OF THE PARAMETERS OF AN EOS

The most common cubic EOS of engineering interest can be written in a generalized form [22], in terms of reduced variables $T_r = T/T_c$,

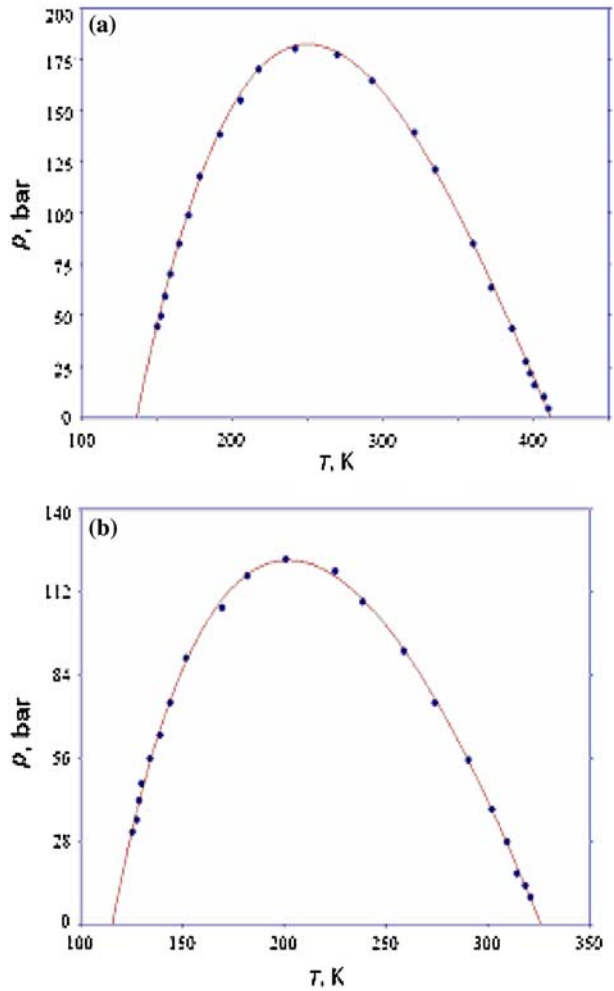

Fig. 6. Calculated points for the BC (•) obtained from empirical equation of (a) Tegeler et al. for Ar [26] and (b) Span et al. [25] for N_2 were fitted into Eq. (13).

$p_r = p/p_c$, and $v_R = p_c v/(RT_c)$, as

$$p_r = \frac{RT_r}{v_R - b} - \frac{a_c \alpha(T_r)}{v_R^2 + k_1 b v_R + k_2 b^2}, \tag{14}$$

where k_1, k_2, the critical cohesion parameter a_c, and the covolume b are characteristic constants of the EOS; e.g., $k_1 = 1$, $k_2 = 0$, $a_c = 0.42$, and

Table IV. Analytical Expressions for the JIC by using given EOSs

EOS	Expressions for the JIC
RK	$a=0$
SRK	$(m+m^2+m^2(T/T_c)^{1/2})T-2T_cm(T/T_c)^{1/2}-T_cm^2(T/T_c)^{1/2}-T_cm^2(T/T_c)^{3/2}$ $-(T/T_c)^{1/2}T_c=0$
LIR	$A_1v^2-B_1=0$
vdW	$a=0$
MLIR	$p=\dfrac{(2b^2RT^3+aRbT^2+(-2bRc+2bA_1)T+B_1-aRc+aA_1)RT(bRT^2-cR+A_1)}{B_1\sqrt{(bRT^2-cR+A_1)B_1}v_c}$

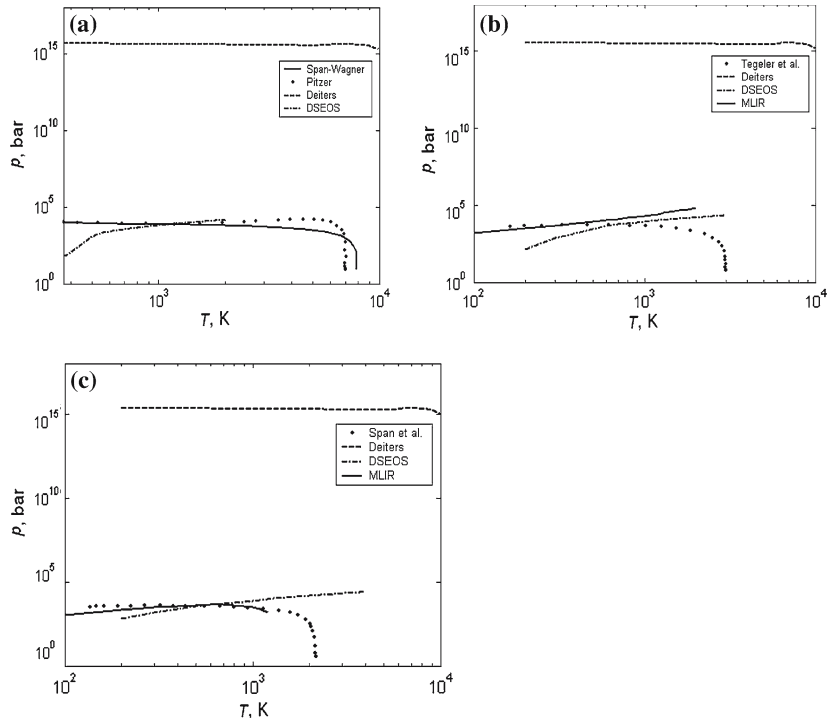

Fig. 7. Predicted JIC given by different EOSs comparing calculations using the empirical EOSs of (a) CO_2 (Pitzer [24] and Span–Wagner [23]), (b) Ar (Tegeler et al. [26]), and (c) N_2 (Span et al. [25]).

$b=0.086$ for the RK EOS; $k_1=0$, $k_2=0$, $a_c=27/64$, and $b=1/8$ for vdW EOS [22]. The cohesion function $\alpha(T_r)$ expresses the temperature dependence of the attraction term. Cubic EOSs are strongly oriented toward vapor–liquid equilibrium applications, e.g., the widely used cohesion function,

$$\alpha=\left[1+m(1-T_r^{1/2})\right]^2 \tag{15}$$

had its origins in the fitting of saturation pressures of pure fluids [33]. Other properties are less well represented in practice. Colina et al. [34] have shown that the extrapolation of an EOS to supercritical temperatures can result in significant errors when computing densities on the critical isochore, the second virial coefficients, and the JTIC.

We developed new cohesion functions for the RK and vdW EOSs and the parameter A_2 in the LIR using a procedure based on the JTIC. For the cubic EOS of Eq. (14), the inversion criterion of Eq. (2) gives a first-order ordinary differential equation for $\alpha(T_r)$ as

$$\frac{T_r a_c}{(v_R^2+k_1 b v_R+k_2 b^2)}\frac{d\alpha(T_r)}{dT_r}-\frac{a_c v_r(2v_r+k_1 b)}{(v_R^2+k_1 b v_R+k_2 b^2)^2}\alpha(T_r)+\frac{bT_r}{(v_R-b)^2}=0. \tag{16}$$

By having the JTIC as a $p(T)$ function, the differential-algebra set of Eqs. (14) and (16) can be solved for T_r and $\alpha(T_r)$, subject to the boundary condition $\alpha(T_r)=1$ for critical-point stability. Since the numerical integration procedure required a continuous representation of the entire JTIC, the data must be fitted with an equation. Among the general empirical equations that have been presented for the JTIC, we selected the Miller equation [Eq. (6)] because it uses a simple form and gives at least good agreement with experimental inversion data of CO_2; see Fig. 2.

The first-order ordinary differential Eq. (16) may be solved by using a seventh/eighth-order continuous Runge–Kutta method. We run the procedure 'dverk78' using Maple. The step size was set to zero. Using this method, we have obtained a new supercritical cohesion function based on CO_2 for the vdW and RK EOSs. The calculated cohesion parameters for the two cubic EOSs are shown in Fig. 8. For $T_r>2.1$, the values of $\alpha(T_r)$ given by the vdW become imaginary, for which its real part is negative, and is not shown in Fig. 8a. According to the vdW EOS, up to $T_r=2.1$, the intermolecular attractions are meaningful. At high temperatures, molecules behave like hard spheres. In other words, only the intermolecular repulsions are important when $T_r>2.1$. The value of $T_r=2.1$ may be compared with the reduced Boyle temperature of CO_2, 2.34 [5]. So the value

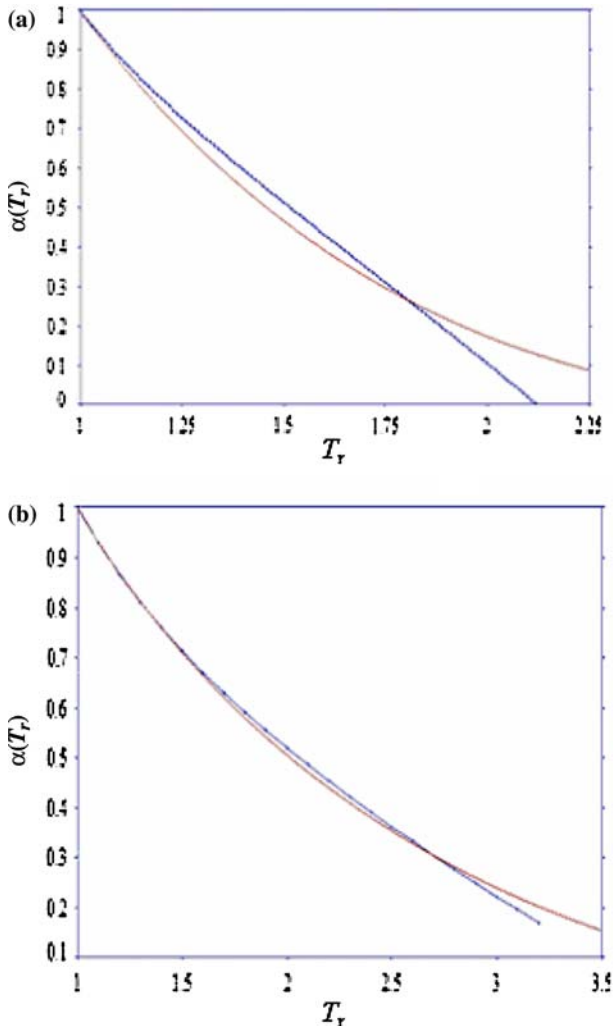

Fig. 8. Cohesion function computed from the Joule–Thomson inversion data for the (a) vdW and (b) RK that were fitted with Eq. (15).

of $\alpha(T_r)$ is reasonable for $T_r > 2.1$. The $\alpha(T_r)$ function, which is positive, is a criterion for the intermolecular attractions and continuously decreases with temperature. Regarding the RK EOS, for the reduced temperature $T_r > 3.3$, the $\alpha(T_r)$ becomes imaginary. Based on this EOS, the calculated Boyle temperature for CO_2 is equal to 2.9 [14], which is comparable to $T_r = 3.3$.

Table V. Values of the Coefficients of the New Cohesion Function of Eq. (17), along with the Correlation Coefficient, R^2

	Coefficients of the Cohesion Function (Eq. (17))				
EOS	m_1	m_2	m_3	m_4	R^2
RK	−7.858	5.846	−2.169	0.2983	1
vdW	−55.04	59.3	−29.02	5.223	1

We have fitted the calculated values of $\alpha(T_r)$, obtained from both vdW and RK EOSs, into the following expression reported by Colina and Olivera-Fuentes [29]:

$$\alpha = 1 + m_1\left(T_r^{1/2} - 1\right) + m_2(T_r - 1) + m_3\left(T_r^{3/2} - 1\right) + m_4\left(T_r^2 - 1\right). \quad (17)$$

The coefficients of Eq. (17) are given in Table V. As shown in Fig. 8, the calculated value of $\alpha(T_r)$ obtained from the vdW and RK EOSs are poorly fitted with the Soave formula, Eq. (15). However, as shown in Table V, the values of $\alpha(T_r)$ are well fitted with Eq. (17) for both EOSs, with a correlation coefficient $R^2 = 1$.

We may now use the new cohesion function to calculate the JTIC, using the vdW and RK EOSs. The results of such calculations for CO_2 are shown in Fig. 9, compared to the results obtained from the original EOSs. So we may conclude that the EOSs with the new cohesion functions give better predictions for the JTIC than the original equations, as long as the temperature is such that the attraction is dominant, i.e., $\alpha(T_r)$ has a real value.

It is interesting to see whether such a modification gives a better prediction for the other ideal curves, as well. To find an answer, we used the RK and MRK to predict the Zeno line, BC, and JIC. On the basis of the MRK, we found the following expression for the Zeno line:

$$[T_r b - a_c\alpha(T_r)]v_r + a_c\alpha(T_r)b + T_r b^2 = 0. \quad (18)$$

The experimental Zeno line for CO_2 is shown in Fig. 10, along with those predicted by the RK and MRK. As shown in this figure, the predicted line given by the MRK is significantly better than that of the RK.

Figure 11 shows the BC given by the MRK and RK in comparison with those obtained from the empirical equations (Span–Wagner and Pitzer) for CO_2. As shown in this figure, the predicted curve given by the

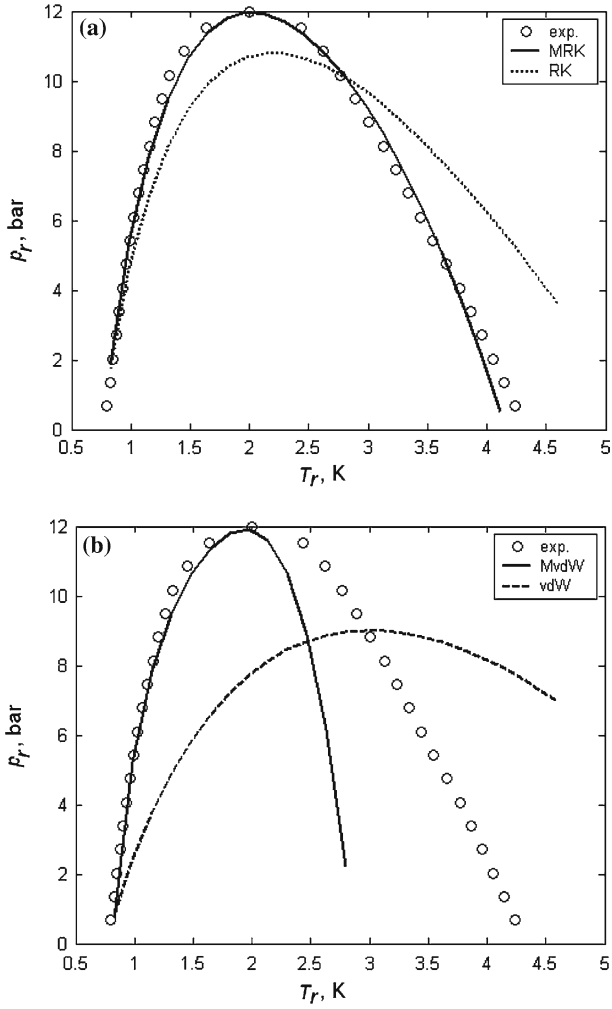

Fig. 9. JTIC for CO_2 computed from (a) RK and (b) vdW EOSs with the new cohesion function of Eq. (17). Calculated results obtained from the original EOSs are also shown for comparison.

MRK is better than that of the RK. Both the MRK and RK give no meaningful curve for the JIC.

Unlike the previous case, we may now consider the repulsion term of the vdW to be temperature dependent, but the attraction term independent

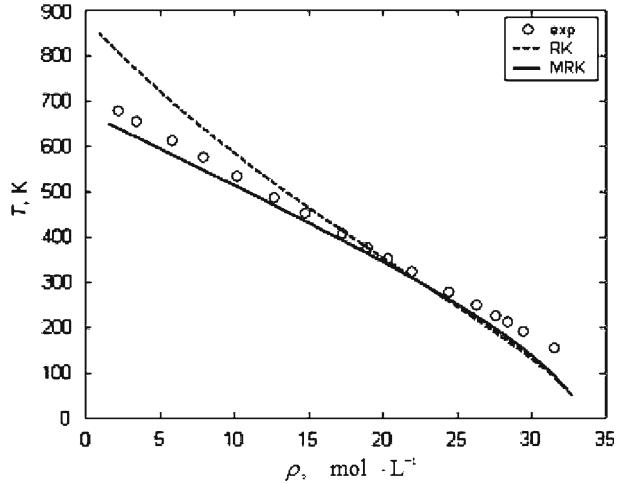

Fig. 10. Predicted T versus ρ given by the RK and MRK EOSs for the $Z = 1$ contour, compared with the experimental Zeno line for CO_2.

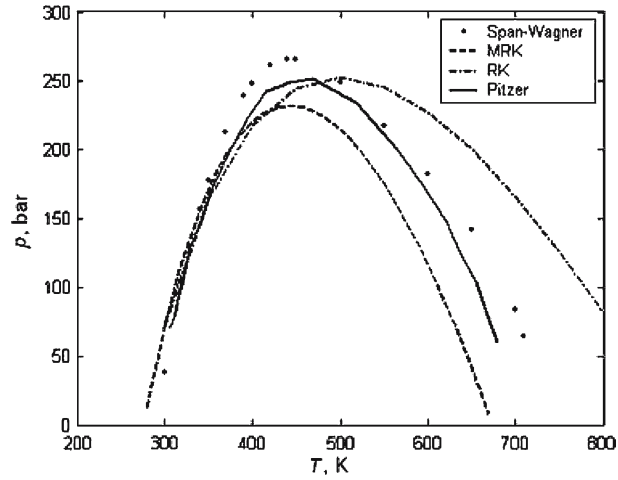

Fig. 11. Predicted BC given by the RK and MRK EOSs for CO_2 compared with those obtained from the empirical equations of Pitzer [24] and Span–Wagner [23].

of temperature. Then Eq. (14) becomes

$$p_r = \frac{RT_r}{v_R - b\beta(T_r)} - \frac{a_c}{v_R^2 + k_1 b v_R + k_2 b^2}. \tag{19}$$

By applying the JTIC condition on Eq. (19), the following differential equation will be obtained:

$$\frac{\nu_R a_c(2\nu_R + k_1 b)}{(\nu_R^2 + k_1 b\nu_R + k_2 b^2)} - \frac{T_r[T_r b(d\beta(T_r)/dT_r) - \nu_R]}{(\nu_R - b\beta(T_r))^2} + \frac{T_r}{(\nu_R - b\beta(T_r))} = 0. \quad (20)$$

Numerical solution of Eq. (20) would give $\beta(T_r)$, which is shown in Fig. 12a.

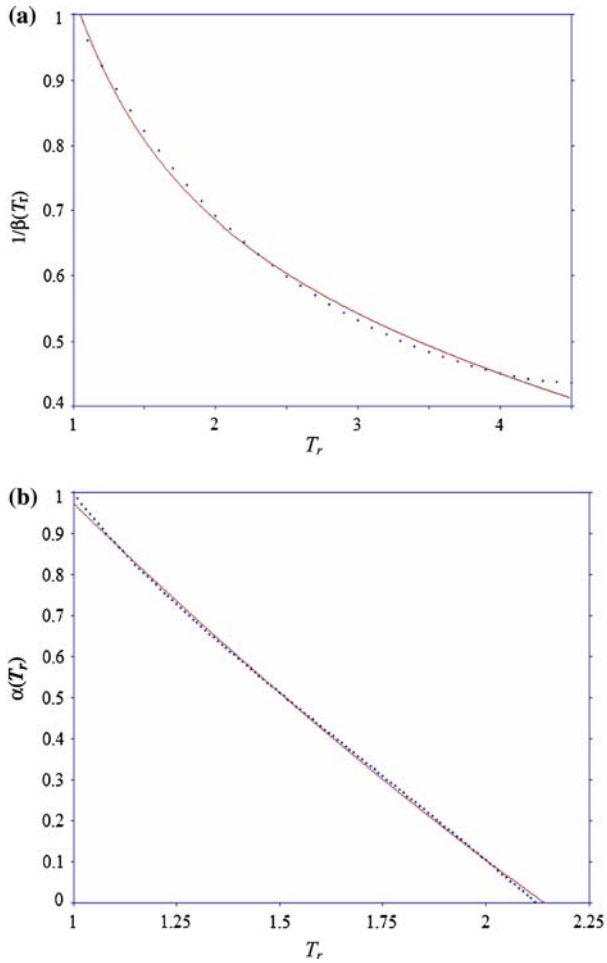

Fig. 12. Calculated values of (a) $\beta(T_r)$ and (b) $\alpha(T_r)$ of the vdW obtained from the JTIC for CO_2 which are well fitted with Eqs. (21) and (22), respectively.

Parsafar and Saydi [10] have recently shown that the deviation given by the vdW EOS for the experimental Zeno line may be due to temperature dependences of the a and b parameters of this EOS. They have found temperature dependences of the a and b parameters in such a way that the EOS gives a more accurate prediction for the Zeno line. They found that

$$\alpha(T_r) = a_0 + a_1 T_r + a_2 T_r^2, \tag{21}$$

$$1/\beta(T_r) = 1/b_0 + b_1 T_r + \frac{b_{-1}}{T_r}. \tag{22}$$

The calculated results for $\alpha(T_r)$ and $\beta(T_r)$ are plotted in Fig. 12 for CO_2, which are well fitted with Eqs. (21) and (22), respectively.

They also have found the temperature dependence of the A_2 parameter in such a way that the LIR can give a linear relation between ρ and T on the $Z=1$ contour as given in Eq. (12). We may use the same approach for the RK and vdW EOSs to find the temperature dependence of A_2 for the LIR. The approach leads to the following differential equation:

$$\frac{dA_2(T)}{dT} = \frac{2A_2(T)}{T} - \frac{3A_1}{RT^2} + \frac{5B_1\rho^2}{RT^2}. \tag{23}$$

We have used the JTIC experimental data of argon to calculate A_2 from Eq. (23). To solve Eq. (23), ρ should be substituted in terms of T. The experimental density of the JTIC had been first fitted with a polynomial function in terms of temperature (with $R^2=1$) as,

$$\rho = a + bT_r + cT_r^2 + dT_r^3 + eT_r^4 + fT_r^5. \tag{24}$$

The function ρ given in Eq. (24) was then substituted into Eq. (23). The numerical solution of the final equation gives $A_2(T)$, which is shown in Fig. 13. As shown in this figure, the calculated values of A_2 are well fitted with Eq. (12), which was obtained on the basis of the $Z=1$ contour [10].

6. DISCUSSION

The accuracies of seven different EOSs have been evaluated numerically in predicting the ideal curves (JTIC, JIC, and BC) in this work. The predictions for the JTIC were compared to experimental data (see Fig. 1).

No experimental data have been reported for the BC and JIC; therefore, the calculated curves from different EOSs have been compared with those calculated from the empirical equations (see Figs. 5 and 7). Among these EOSs, the Deiters EOS shows the best agreement overall. However, none of them can predict the upper temperature branch with a reasonable

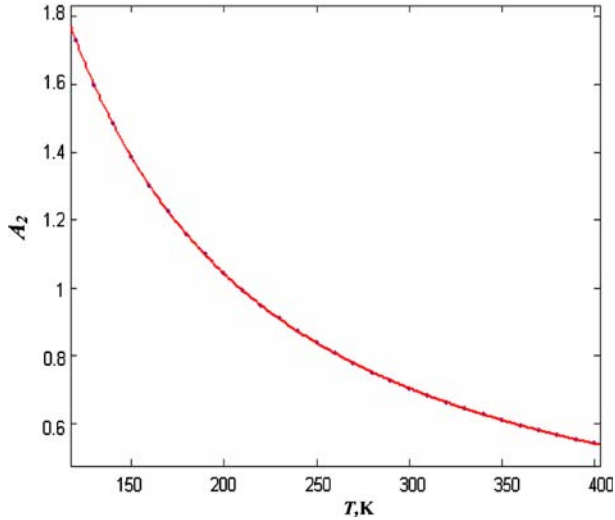

Fig. 13. Temperature dependence of the A_2 parameter of the LIR calculated on the basis of the JTIC for argon, which is well fitted with Eq. (12).

accuracy. As explained in the text, the reason is that an EOS (like RK) gives the minimum of the Z versus T for an isobar more accurately than the maximum (see Fig. 4a, b).

We have been able to obtain analytical expressions for the JTIC and BC only by using the LIR, MLIR, and vdW EOSs. The expression from the LIR is the simplest (see Figs. 2 and 6). The experimental data for the JTIC are well fitted with the derived expression given by the LIR in such a way that the fitting is better than those of the empirical expressions given by Gunn et al. [21] and Miller [13]. Also, a similar expression for the BC was obtained from the LIR for which the calculated points from the empirical EOSs of Tegeler et al. [26] for Ar and of Span et al. [25] for N_2 are well fitted.

The calculated JIC from different EOSs show that none of them give a reasonable prediction; only the MLIR, Deiters, and DSEOS equations give non-trivial expressions for the curve. The MLIR gives the best prediction (see Fig. 7).

On the basis of the JTIC, an approach is given for obtaining the temperature dependence of EOS parameters. Such an approach has been used to determine the temperature dependences of A_2 of the LIR (see Fig. 13), a and b parameters of the vdW (see Figs. 8a and 12), and the cohesion

function of the RK (see Fig. 8b). We have found that such temperature dependences obtained on the basis of the JTIC are appropriate for the other ideal curves as well (see Figs. 10 and 11).

We may also investigate the impact of the temperature dependence of A_2 on other regularities. If A_2 is assumed to be independent of temperature, then two common intersection points (namely, the common bulk modulus and common compression point) were found to be independent of temperature [36]. However, if A_2 depends on temperature as given by Eq. (12), the intersection points would be temperature dependent. For instance, the density of the common compression point, ρ_{oz}, may be obtained as

$$\rho_{oz}^2 = \frac{A_1}{B_1} + \frac{bRT^2 - cR}{B_1}$$

for which the second term makes ρ_{oz} to be weakly temperature dependent, which is in accordance with experiment [37].

ACKNOWLEDGMENT

We acknowledge the Sharif University of Technology Research Council for financial support.

APPENDIX: DETAILS OF EOSs

1. Redlich–Kwong (RK)

$$p = \frac{RT}{v-b} - \frac{a}{T^{1/2}v(v+b)}$$
$$a = \Omega_a \frac{R^2 T_c^{2.5}}{p_c}$$
$$\Omega_a = 0.42747$$
$$b = \Omega_b \frac{RT_c}{p_c}$$
$$\Omega_b = 0.08670$$

2. Soave–Redlich–Kwong (SRK)

$$p = \frac{RT}{v-b} - \frac{a}{v(v+b)}$$
$$b = 0.08664\frac{RT_c}{p_c}$$
$$a = \beta\alpha(T)$$
$$\alpha(T) = \left[1 + m\left(1 - \sqrt{T_r}\right)\right]^2$$
$$\beta = a_c\frac{R^2T_c^2}{p_c}$$
$$a_c = 0.4274$$
$$m = 0.480 + 1.574\omega - 0.176\omega^2$$

3. Deiters EOS

$$p = \frac{RT}{v}\left[1 + CC_0\frac{4\eta - 2\eta^2}{(1+\eta)^3}\right] - \frac{abR\tilde{T}_{\text{eff}}}{v^2}\left[\exp\left(\frac{1}{\tilde{T}_{\text{eff}}}\right) - 1\right] I_1(\tilde{p})$$
$$\eta = (\pi/6)\sigma^3 N_A/v$$
$$\tilde{p} = b/v$$
$$\tilde{T} = CT/a$$
$$\tilde{T}_{\text{eff}} = (\tilde{T} - 0.06911C\tilde{p})/y$$
$$I_1(p) = (\gamma/C)^2\sum_{k=0}(k+1)h_k\gamma^k p^k$$
$$\gamma = 1 + 0.697816(C-1)^2$$
$$h_0 = 7.0794046, \quad h_1 = 12.08351455, \quad h_2 = -53.6059$$
$$h_3 = 143.6681, \quad h_4 = -181.1554682, \quad h_5 = 78.5739255$$
$$y(\tilde{p}) = f^2 - C^{-5.5}f(1-f) + (1 - 0.65/c)(1-f)^2$$
$$f = \exp\left[CC_0(3\eta^2 - 4\eta)/(1-\eta)^2\right]$$
$$C_0 = 0.6887$$
$$\gamma = 0.06911C$$
$$a = \varepsilon/k_B$$
$$b = N_A\sigma^3/2^{1/2}$$

4. Linear isotherm regularity (LIR)

$$(Z-1)\left(\frac{v}{v_c}\right)^2 = A + B\left(\frac{\rho}{\rho_c}\right)^2$$

$$A = A_2 - \frac{A_1}{RT}$$

$$B = \frac{B_1}{RT}$$

5. Modified linear isotherm regularity (MLIR)

$$A_2 = a + bT + c/T$$

6. Dense system equation of state (DSEOS)

$$p_r v_r^2 = A_0 + A_1\rho_r + A_2\rho_r^2$$

$$A_i = a_i + b_i T + c_i T\ln(T)$$

7. van der Waals (vdW)

$$\left(p + \frac{a}{v^2}\right)(v-b) = RT$$

REFERENCES

1. R. Span and W. Wagner, *Int. J. Thermophys.* **18**:1415 (1997).
2. E. H. Brown, *Bull. Int. Inst. Refrig. Annexe* **1:**169 (1960).
3. K. M. De Reuck, *Report PC/D45/1*, IUPAC Thermodynamic Tables Project Centre, London (1991).
4. A. Batschinski, *Ann. Phys.* **19**:307 (1906).
5. J. Xu and D. R. Herschbach, *J. Phys. Chem.* **96:**2307 (1992).
6. M. Holeran, *J. Phys. Chem.* **72**:1230 (1968).
7. M. Holeran, *J. Phys. Chem.* **73**:167 (1969).
8. M. Holeran, *Ind. Eng. Chem. Res.* **29**:632 (1990).
9. M. Holeran, *J. Phys. Chem.* **49**:39 (1968).
10. G. A. Parsafar and H. Saydi, *Int. J. Thermophys.* **25**:1819 (2004).
11. I. Polishuk and J. H. Vera, *J. Phys. Chem. B* **109**:5977 (2005).
12. G. W. Dilay and R. A. Heidemann, *Ind. Eng. Chem. Fundam.* **25**:152 (1986).
13. D. G. Miller, *Ind. Eng. Chem. Fundam.* **9**:585 (1970).
14. U. K. Deiters and K. M. De Reuck, *Fluid Phase Equilib.* **161**:205 (1999).
15. K. Juris and L. A. Wenzel, *AIchE J.* **18**:648 (1972).
16. N. A. Darwish and S. A. Al-Muhtaseb, *Thermochim. Acta* **287**:43 (1996).
17. A. Maghari and N. S. Matin, *J. Chem. Eng. Jpn.* **30**:520 (1997).
18. S. Alavi, G. A. Parsafar, and B. Najafi, *Int. J. Thermophys.* **16**:1421 (1995).
19. D. M. Heyes and C. T. Liaguno, *Chem. Phys.* **168**:61 (1992).
20. C. M. Colina, M. Lísal, F. R. Siperstein, and K. E. Gubbins, *Fluid Phase Equilib.* **202**:253 (2002).

21. R. D. Gunn, P. L. Chueh, and J. M. Prausnitz, *Cryogenics* **6**:324 (1966).
22. M. G. Castillo, C. M. Colina, J. E. Dubuc, and C. G. Olivera-Fuentes, *Proc. 7th Brazilian Congress of Engineering and Thermal Science*, ENCIT 98, Rio de Janeiro, Brazil (1998).
23. R. Span and W. Wagner, *J. Phys. Chem. Ref. Data* **25**:1509 (1996).
24. K. S. Pitzer and Sterner, *Int. J. Thermophys.* **16**:511 (1995).
25. R. Span, E. W. Lemmon, R. T Jacobson, W. Wagner, and A. Yokozeki, *J. Phys. Chem. Ref. Data* **29**:1361 (2000).
26. C. Tegeler, R. Span, and W. Wagner, *J. Phys. Chem. Ref. Data* **28**:779 (1999).
27. G. A. Parsafar, F. Kermanpour, and B. Najafi, *J. Phys. Chem. B* **103**:7283 (1999).
28. G. A. Parsafar and F. Kermanpour, *Int. J. Thermophys.* **22**:1795 (2001).
29. C. M. Colina and C. Olivera-Fuentes, *Ind. Eng. Chem. Res.* **41**:1064 (2002).
30. R. H. Perry and D. W. Green, eds., *Perry's Chemical Engineers Handbook*, 7th Ed. (McGraw-Hill, New York, 1997). Sect. 2, pp. 132–139.
31. V. P. S. Nain and R. A. Aziz, *Can. J. Chem.* **54**:2617 (1976).
32. E. Keshavarzi, G. A. Parsafar, and B. Najafi, *Int. J. Thermophys.* **20**:643 (1999).
33. G. Soave, *Chem. Eng. Sci*. **27**:1197 (1972).
34. C. M. Colina, J. W. Santos, and C. Olivera-Fuentes, *High Temp.-High Press.* **29**:525 (1997).
35. *NIST Chemistry Webbook*, http:/www.Webbook (Nat. Inst. Stds. Technol., Gaithersburg, Maryland, 2006).
36. B. Najafi, G. A. Parsafar, and S. Alavi, *J. Phys. Chem.* **99**:9248 (1995).
37. A. Boushehri, F.-M. Tao, and E. A. Mason, *J. Phys. Chem.* **97**:2711 (1993).